Coherent signature of warming-induced extreme sub-continental boreal wildfire activity 4800 and 1100 years BP

Environmental Research Letters

LETTER

Coherent signature of warming-induced extreme sub-continental boreal wildfire activity 4800 and 1100 years BP

Martin P Girardin[1,2,10,11], **Jeanne Portier**[2,3,10], **Cécile C Remy**[4,5,6], **Adam A Ali**[4,5], **Jordan Paillard**[4,7], **Olivier Blarquez**[7], **Hugo Asselin**[8], **Sylvie Gauthier**[1,2], **Pierre Grondin**[9] **and Yves Bergeron**[2,4]

[1] Natural Resources Canada, Canadian Forest Service, Laurentian Forestry Centre, 1055 du PEPS, PO Box 10380, Stn. Sainte-Foy, Québec, QC, G1V 4C7, Canada
[2] Centre for Forest Research, Université du Québec à Montréal, PO Box 8888, Stn. Centre-ville, Montréal, QC, H3C 3P8, Canada
[3] Forest Resources and Management, Swiss Federal Institute for Forest, Snow and Landscape Research WSL, Zürcherstrasse 111, 8903 Birmensdorf, Switzerland
[4] Forest Research Institute, Université du Québec en Abitibi-Témiscamingue and Université du Québec à Montréal, 445 boul. de l'Université, Rouyn-Noranda, QC, J9X 5E4, Canada
[5] Institut des Sciences de l'Evolution—Montpellier, UMR 5554 CNRS-IRD-Université Montpellier-EPHE, Montpellier, France
[6] Department of Biology, 1 University of New Mexico, Albuquerque, New Mexico, 87131-0001, United States of America
[7] Département de Géographie, Université de Montréal, Pavillon 520 Chemin-de-la-Côte-Ste-Catherine, Montréal QC, H2V 2B8, Canada
[8] School of Indigenous Studies, Université du Québec en Abitibi-Témiscamingue, 445 boul. de l'Université, Rouyn-Noranda, QC, J9X 5E4, Canada
[9] Direction de la recherche forestière, Ministère des Forêts, de la Faune et des Parcs du Québec, 2700 Einstein, Québec, QC, G1P 3W8, Canada
[10] Authors contributed equally to the work.
[11] Author to whom any correspondence should be addressed.

E-mail: martin.girardin@canada.ca

OPEN ACCESS

RECEIVED
29 May 2019

REVISED
7 November 2019

ACCEPTED FOR PUBLICATION
20 November 2019

PUBLISHED
9 December 2019

Keywords: Boreal forest, sedimentary charcoal, climate change, paleoecology, temperature

Supplementary material for this article is available online

Abstract

Climate changes are expected to progressively increase extreme wildfire frequency in forests. Finding past analogs for periods of extreme biomass burning would provide valuable insights regarding what the effects of warming might be for tree species distribution, ecosystem integrity, atmospheric greenhouse gas balance, and human safety. Here, we used a network of 42 lake-sediment charcoal records across a ~2000 km transect in eastern boreal North America to infer widespread periods of wildfire activity in association with past climate conditions. The reconstructed fluctuations in biomass burning are broadly consistent with variations in ethane concentration in Greenland polar ice cores. Biomass burning fluctuations also significantly co-varied with Greenland temperatures estimated from ice cores, at least for the past 6000 years. Our retrospective analysis of past fire activity allowed us to identify two fire periods centered around 4800 and 1100 BP, coinciding with large-scale warming in northern latitudes and having respectively affected an estimated ~71% and ~57% of the study area. These two periods co-occurred with widespread decreases in mean fire-return intervals. The two periods are likely the best analogs for what could be anticipated in terms of impacts of fire on ecosystem services provided by these forests in coming decades.

Introduction

The Northern Hemisphere has recently experienced extreme wildfire seasons, which have burned extensive forest areas across the boreal biome. Notably, record-breaking warm and dry conditions during the summer of 2018 spurred historic wildfire outbreaks in Sweden, ranging across more than 24 310 ha of lands from north of the Arctic Circle to the southernmost county of Scania (San-Miguel-Ayanz et al 2019). The province of British Columbia, Canada, faced the worst wildfire year on record during the summer of 2017, with 1.2 million ha having burned (Ansmann *et al* 2018, Hu *et al* 2019, Natural Resources Canada 2018). During the summer of 2010, intense drought and high temperatures caused several hundred wildfires in Russia, resulting in about 5 million hectares of burnt areas (Viatte *et al* 2013). Such extreme fire activity can

have important economic and social consequences, especially when it occurs in populated areas. Communities must face evacuations, mental and physical health problems, damage to infrastructure, and disruptions to business and industry (Bowman *et al* 2011, Viatte *et al* 2013, Landis *et al* 2018). As an example, the 590 000 ha Fort McMurray Horse River wildfire in Alberta (Canada) during 2016 incurred the worst insured losses in Canadian history, destroying 2400 buildings (Statistics Canada 2017, Sankey 2018). Again in Canada, massive wildfires during the summer of 2013 threatened a Cree community in northern Quebec, forcing its evacuation (Erni *et al* 2017, Sankey 2018).

Human-caused climate changes, associated with warming and drying at high-latitudes, are expected to progressively increase the frequency of such extreme wildfires in the future, with important consequences for species distribution, ecosystem integrity, atmospheric greenhouse gas balance, and human safety (Flannigan *et al* 2009, Oris *et al* 2014, Gauthier *et al* 2015). Fire suppression agencies will be increasingly overwhelmed (Bowman *et al* 2017, Wotton *et al* 2017). Recently, an analysis of fire weather climatology from 1979 to 2015, which used the North American Regional Reanalysis dataset and the Canadian Fire Weather Index System, has suggested an ongoing significant, increasing trend in fire-season length in eastern Canada (Jain *et al* 2017). To date, detection of temporal changes in the frequency (or in the return interval) of major wildfire activity remains a major challenge, owing to the short temporal coverage of circumboreal fire data (usually limited to post-1950), the large interannual and spatial variability in area that is burned, and evolving wildfire monitoring and reporting methods, which tend to mask long-term and subtle changes that can be a consequence of changing climate (Krezek-Hanes *et al* 2011, Waito *et al* 2015). The need for a comprehensive assessment of historical wildfire, climate, and vegetation at all scales, including enhanced datasets from historical fire maps and synthesis of climate, vegetation, and fire interactions from past climates, including past warm periods, was identified as national priorities for building the capacity of wildland fire science in the 2020s (Sankey 2018).

Lake-sediment charcoal records are used to reconstruct long-term fire trends and analyze the sensitivity of fire activity to various ecosystem and climatic processes, and can ultimately improve our ability to project future fire impacts (Heyerdahl *et al* 2008, Girardin *et al* 2013b, Waito *et al* 2018). Charcoal particles that are produced during fire are transported by wind and runoff across landscapes and deposited in lake sediments. They have been used to infer trends in typical (average) biomass burning and changes in fire-return intervals (FRIs) from local to hemispheric scale (Marlon *et al* 2012, Pellatt *et al* 2015, Waito *et al* 2015, 2018). Here we extend the utility of these records by demonstrating their applicability in distinguishing synchronous fires or fire periods at the sub-continental scale in an attempt to link widespread pulses of biomass burning and rapid warming during pre-industrial times. We illustrate our case with the use of a network of 42 lake-sediment charcoal records that cover the last 8400 years in central and eastern boreal North America. The retrospective analysis of past fire activity allowed us to identify signals from two high-fire activity periods across the study area, dating from about 4800 and 1100 calibrated years before present (BP), and having occurred during climatic warming at high latitudes.

Data and methods

Forest fire data

Charcoal samples from 42 lake sediment cores were obtained from 14 studies sharing a common protocol of charcoal extraction (see the references listed in table S1 for details, and figure S1 is available online at stacks.iop.org/ERL/14/124042/mmedia for study locations). The network extends throughout the eastern North American boreal forest across a west-to-east transect of more than 2000 km, which covers three Canadian provinces (figure 1(a); table S1). Forests in this area developed during the Holocene, which began with the end of the most recent glaciation about 11 650 years BP (Dyke 2004, Walker *et al* 2018). During this period, ice sheet margins retreated northeastward. As the glacier retreated, and following the disappearance of the proglacial Objibway Lake ca. 8200 BP, forest density increased with fire-adapted conifer tree species *Picea* becoming, and remaining, the dominant feature in boreal landscapes; together with *Abies*, broadleaved trees such as *Acer* were dominant in the mixedwood forests south of the study area (figure S2; Blarquez *et al* 2015). The average length of the sediment cores was 320 cm (table S1); in most cases, sampling had reached the contact between organic and mineral sediments, allowing fire histories to be traced back to the very beginning of the post-glacial afforestation period. All cores were sliced at contiguous 0.5 or 1.0 cm intervals to discern fire events at high temporal resolution. The analysis of a network of fire activity records of this magnitude allowed us to achieve unequaled spatial and temporal resolution in this part of North America (i.e. Girardin *et al* 2013a, Blarquez and Aleman 2016). Sediment accumulation chronologies were generated based on AMS radiocarbon dating of terrestrial plant macroremains and bulk gyttja samples, and ^{210}Pb when available (table S1). ^{210}Pb measurements were performed from the uppermost 10–20 cm of the cores. ^{210}Pb values were inferred by measuring the activity of the daughter product, ^{210}Po, by alpha spectrometry assuming an equal concentration between the two isotopes. The ^{210}Pb concentrations were interpreted using the constant rate of supply model of ^{210}Pb accumulation (Appleby and Oldfield 1978). ^{14}C dates

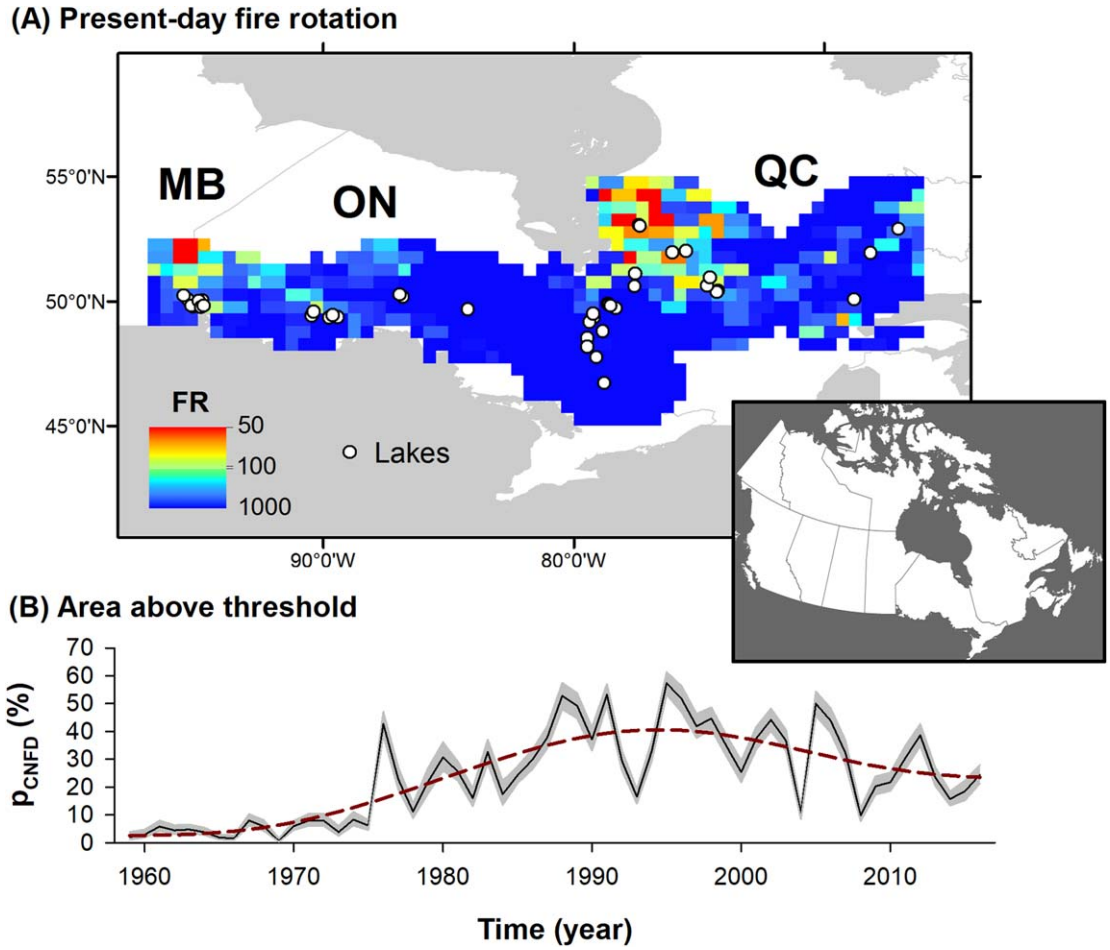

Figure 1. (a) Distribution of the sampled lakes (circles) within the 0.5° × 0.5° study grid in eastern boreal North America. The background color illustrates the fire rotation (FR) for each cell that was computed for the 1959–1999 period using national fire data (data from Boulanger *et al* 2014). (b) Proportion of cells in which the annual sum of area that burned (human- and lightning ignited) exceeded the locally-defined extreme detection threshold, computed using data from the Canadian National Fire Database (hereafter, $\hat{p}_{CNFD}$), with 95% confidence intervals (shaded). A high $\hat{p}_{CNFD}$ denotes a year during which biomass burning occurred across an extensive area. The dashed line is a 10 year window second-order polynomial smoothing. Canadian provinces under study: Manitoba (MB), Ontario (ON), and Quebec (QC).

were calibrated using Bayesian models (Parnell *et al* 2008; Bchron R package) or 'classical' models (Blaauw 2010; CLAM 2.2 program) based on the IntCal13.14 C data set, as presented in original studies (Hua *et al* 2013, Reimer *et al* 2013). It has been shown that the two models (Bayesian and 'classical') derive relatively equivalent chronologies (Blaauw 2010) for the studied time period (0–8450 BP; Wang *et al* 2019) and lakes (figure S3). Charcoal particles were measured and the resulting data were converted into charcoal accumulation rates ($CHAR_{raw}$; $mm^2\ cm^{-2}\ yr^{-1}$) that were based on numerical age-depth models to reconstruct past fire frequencies for each lake (table S1). The dates of local fire events were extracted from the $CHAR_{raw}$ series using CharAnalysis v1.1 software (Higuera *et al* 2010). $CHAR_{raw}$ series were interpolated ($CHAR_{interpolated}$) to equal time steps based on the median time-resolution computed from the sediments for each lake (table S1). $CHAR_{interpolated}$ series were decomposed into a low-frequency component ($CHAR_{background}$) and a high-frequency component ($CHAR_{peak}$). $CHAR_{background}$ results from long-distance burning or redeposition processes of charcoal particles that are unrelated to local fire occurrences. $CHAR_{background}$ was estimated by applying the LOWESS-smoother robust technique, and subtracted to $CHAR_{interpolated}$ to obtain the $CHAR_{peak}$ component. $CHAR_{peak}$ was decomposed into two sub-populations: $CHAR_{noise}$ representing variability in sediment mixing and sampling, together with analytical and naturally occurring noise; and $CHAR_{fire}$ representing significant charcoal peaks (Gavin *et al* 2006, Higuera *et al* 2010). For each peak, we used a Gaussian mixture model to identify the $CHAR_{noise}$ distribution according to a locally-defined threshold. Signal-to-noise indices (Kelly *et al* 2011) and goodness-of-fit (Brossier *et al* 2014) were used to evaluate the effectiveness of the discrimination between $CHAR_{fire}$ and $CHAR_{noise}$ and to assess peak detection accuracy by comparing the empirical and fitted noise distributions, respectively (figure S4). Each $CHAR_{peak}$ that exceeded the threshold at the 99th percentile of the noise distribution was assumed to originate from a local fire event (Gavin *et al*

2006, Higuera *et al* 2011). Given the short fire rotations in some parts of the study area (e.g. northwestern Quebec, figure 1), we recognize that some peaks may include more than one fire (Higuera *et al* 2011).

Forest fire data from the Canadian National Fire Database (Stocks *et al* 2002) were used for this study to described current fire activity. The database contains information on the location, date of detection, size (ha), and cause (lightning or human) of all fires that were recorded in Canada, for the period 1959–2016. Starting from the 0.5° × 0.5° grid covering the study area (figure 1), we extracted all fires and computed the annual area burned for each cell and year.

FRI and biomass burning

FRI is herein defined as the time that has elapsed between two successive fires that are deduced from $CHAR_{fire}$, and which are assumed to have occurred within a given landscape area. For each lake, fire dates were converted to FRIs by subtracting each date from the previous one.

$CHAR_{raw}$ series were submitted to a *min–max* normalization to remove biases that could result from differences in taphonomic processes between lakes. Normalized charcoal accumulation ($CHAR_{norm}$) was used as a proxy for biomass burning (Blarquez *et al* 2015). All FRI and $CHAR_{norm}$ series were extended at both edges using a mirror reflection method in order to cover the beginning and the end of each series.

Weibull smoothing

To avoid overestimating the importance of single fire events, the FRI distributions were smoothed independently for each lake using the two-parameter Weibull probability density distribution (Johnson and Gutsell 1994, Cyr *et al* 2009) and a 5-observation moving window. The *b* and *c* parameters, which respectively corresponded to the shape and scale parameters of the Weibull distribution, were estimated using the *fitdist* function of the 'fitdistrplus' *R* package (Delignette-Muller and Dutang 2015). For each lake, we used a gamma (Γ) function (Johnson and Gutsell 1994) to calculate the mean of the Weibull distribution, where within each 5-observation window, the mean FRI was calculated as:

$$\text{Mean FRI} = b\Gamma\left(\frac{1}{c} + 1\right). \quad (1)$$

Bootstrap replications (1000 iterations) were used to construct equi-tailed (1–2σ) confidence intervals for the estimated mean FRI within each window. For each window, the mean of the 1000 resulting values was defined as the Weibull-modeled mean FRI. Weibull-modeled mean FRIs were then reported along the time series for each lake (Cyr *et al* 2009).

Kriging

Ordinary kriging (Cressie 1990) was used to spatially extrapolate changes in FRI and $CHAR_{norm}$ during the Holocene to the entire study area at a 0.5° × 0.5° resolution. Kriging is a linear approach to interpolation/extrapolation of responses, where values across the field surface are determined in accordance with a given covariance structure, which is determined from those observations that are present (Cowtan and Way 2014). The reconstructed values vary smoothly and match the observed values at the coordinates of the observations; they approach the global mean as the distance from the nearest observation increases.

For each lake, values of the Weibull-modeled mean FRI and of the $CHAR_{norm}$ were extracted at a 50 year time resolution from the corresponding distributions. A buffer with a 250 km radius was established around the lakes to delimit the perimeter of the study area, upon which a 0.5° × 0.5° grid was superimposed. This process was repeated at each time step as the pool of lakes changed with time. Ordinary kriging was realized with nugget = 0 and range = 150 km, which were kept constant between time steps. The sill parameter was left unspecified in order for the algorithm to optimize its value at each time step. An exponential model was used to fit the semivariograms. Kriging was performed using the *autoKrige* function of the 'automap' R package (Hiemstra 2009). The resulting FRI_{krig} (which approximates the average FRI, in years, for a specific grid cell during a specific time period) and $CHAR_{krig}$ grids were produced at a 50 year time resolution, and mapped at a 500 year time resolution.

For each 50 year time point, the mean value of all grid cells, along with the corresponding 95% confidence interval, were extracted and reported along the time series to produce the temporal variability of FRI_{krig} and $CHAR_{krig}$. To do so, we examined the local spatial structure of each 50 year time point by using Moran's I spatial correlograms (*moran.test* function; R Core Team 2014), and calculated 95% confidence interval after correcting for the effective degrees of freedom ($n^{\wedge}$) based on lag 1 autocorrelation estimates of Moran's I (see Dale and Fortin 2002). The advantage of averaging the values of the grid cells, rather than the values of the lakes, is that regions where more lakes were sampled were not over-represented.

Extreme biomass burning detection

Extreme biomass burning was defined as periods during which $CHAR_{krig}$ exceeded a detection threshold that was computed from the long-term median (MED) and the median of absolute distances to the median (MAD):

$$x_{(i)} > \text{MED}_{(x)} + z\ \text{MAD}_{(x)}, \quad (2)$$

with $i = 1, \ldots, n$, for a grid-cell's $CHAR_{krig}$ record x of size n time points (Hampel 1985) (figures S5 and S6). The parameter z is a threshold that was selected. The

number of extreme events under analysis was arbitrarily set to approximate the highest 15th percentile (a function of the distance to the median z, which varies by increments of 0.5). For this study, we set $z = 3$. We preferred to use this extreme event detection method on $CHAR_{krig}$ records rather than using local fire events that were detected using CharAnalysis software. Major fires that were identified by $CHAR_{raw}$ peak records can lag actual fire dates by several decades; this is a common occurrence that is related to the timing of charcoal transport and deposition (Higuera *et al* 2005). The fire events are therefore diluted over time, making the interpolation technique unreliable for such identification of individual events as it averages over noise present in their timing. Alternatively, exceedance of the detection $CHAR_{krig}$ threshold indicates high inputs of $CHAR_{raw}$ into a lake, but does not inform on the occurrence of a single fire.

The sample proportion $\hat{p}$, representing the fraction of grid cells k (an integer $\geqslant 0$) of a given population n' (an integer > 0) that was identified positively as recording an extreme event, was computed for each sampled 50 year period from 8450 to 0 years BP. Binomial proportion confidence intervals (95% CIs) were computed using a Bayesian calculation with an uninformative prior distribution (Brown *et al* 2001). This uncertainty estimate is important since n' is unevenly distributed in time, and because small n' or values of k that are close to 0 or 1 can lead to large errors in the estimation of $\hat{p}$. The Bayesian approach that was used here (Jeffreys prior with Beta [1/2, 1/2]) has been shown to be particularly robust under small samples sizes, while also being well-suited for uncertainty estimation under large sample sizes.

The extreme event detection method was repeated on modern area burned data that were extracted from the Canadian National Fire Database, and for each cell over the 1959–2016 period. A year in a given grid cell was deemed as being extreme when the sum of its area burned exceeded the detection threshold set by equation (1) for the particular annual area burned dataset for that particular cell.

Relationship with temperature and Greenland ethane levels

Seasonally unbiased and physically constrained Greenland Summit temperatures that covered the Holocene period, and which were inferred from argon and nitrogen isotopes in air trapped within a Greenland ice core (GISP2; Kobashi *et al* 2017), were used to infer associations between high-latitude temperature variability and biomass burning over the period 8400–0 BP. The Greenland temperature reconstruction has been shown to be representative of hemispheric signals (Kobashi *et al* 2017). It should be noted that sampling density was not constant through the Holocene, such that uncertainty ranges of the reconstructed temperatures varied with time (Kobashi *et al* 2017). The relationship between paleoatmospheric ethane in Greenland polar ice cores (Nicewonger *et al* 2018) and biomass burning was also examined.

Relationships between variables under study were examined using non-parametric stationary bootstrapped correlations (Mudelsee 2003) and wavelet coherence (WTC) analyses (Grinsted *et al* 2004). All analyses accounted for the presence of serial autocorrelation in time series when testing for significance of relationships. The non-parametric stationary bootstrapped correlation technique resamples blocks of data pairs to account for the presence of serial (auto-) correlation in the time series. The confidence intervals (CI) allow testing whether the correlation between two serially dependent time series is significant. When the confidence interval contains zero, the hypothesis of 'no correlation' cannot be rejected at the 95% level. Where indicated, data were ranked prior to analysis to satisfy normality requirements for the correlation analysis. In contrast, WTC examines the significance and magnitude of coherence (i.e. correlation) between two time series and, furthermore, reveals information about the phase relationship (delays) in a lag-period space (at a time and frequency localization). This analysis of phase relationships is relevant in a context in which the direct correlations between variables may be difficult to assess due to dating uncertainties and offset paleorecords. For each time-series, the required frequency spectrum was constructed using continuous wavelet transform analysis. We used the Paul wavelet (order 4) as it is not very localized in frequency space, while allowing signals that are relatively aperiodic to be detected by the analysis (Moore *et al* 2007). The statistical significance level (90%) of the WTC against red noise backgrounds was estimated using Monte Carlo generated noise with 1000 surrogate data set pairs (having the same first-order autocorrelation coefficients as the input datasets; see Grinsted *et al* 2004). WTC was executed using the R package 'biwavelet' version 0.20.11 (Gouhier *et al* 2018). For the purposes of the correlation and WTC analyses, the paleoclimate data were resampled to a lower resolution of 50 year-time steps that was compatible with the CHAR records, using spline estimation; for the correlation with ethane levels in Greenland, biomass burning data were resampled to the time resolution of the ethane data (Software Autosignal).

In our next step in the analysis, spatial correlation maps (Von Storch and Zwiers 1999) were created by analysing the relationship between biomass burning, as computed from modern fire statistics, and gridded temperature data from the Climate Research Unit (CRU TS 4.2 data, resolution of 0.5° latitude × 0.5° longitude). Temperature data were averaged at the grid level over the April–September season. These analyses were conducted using the KNMI Climate Explorer online research tool; all data were ranked prior to analysis (van Oldenborgh *et al* 2008). Additionally, spatial correlation maps were created after analysing the relationship between the Greenland

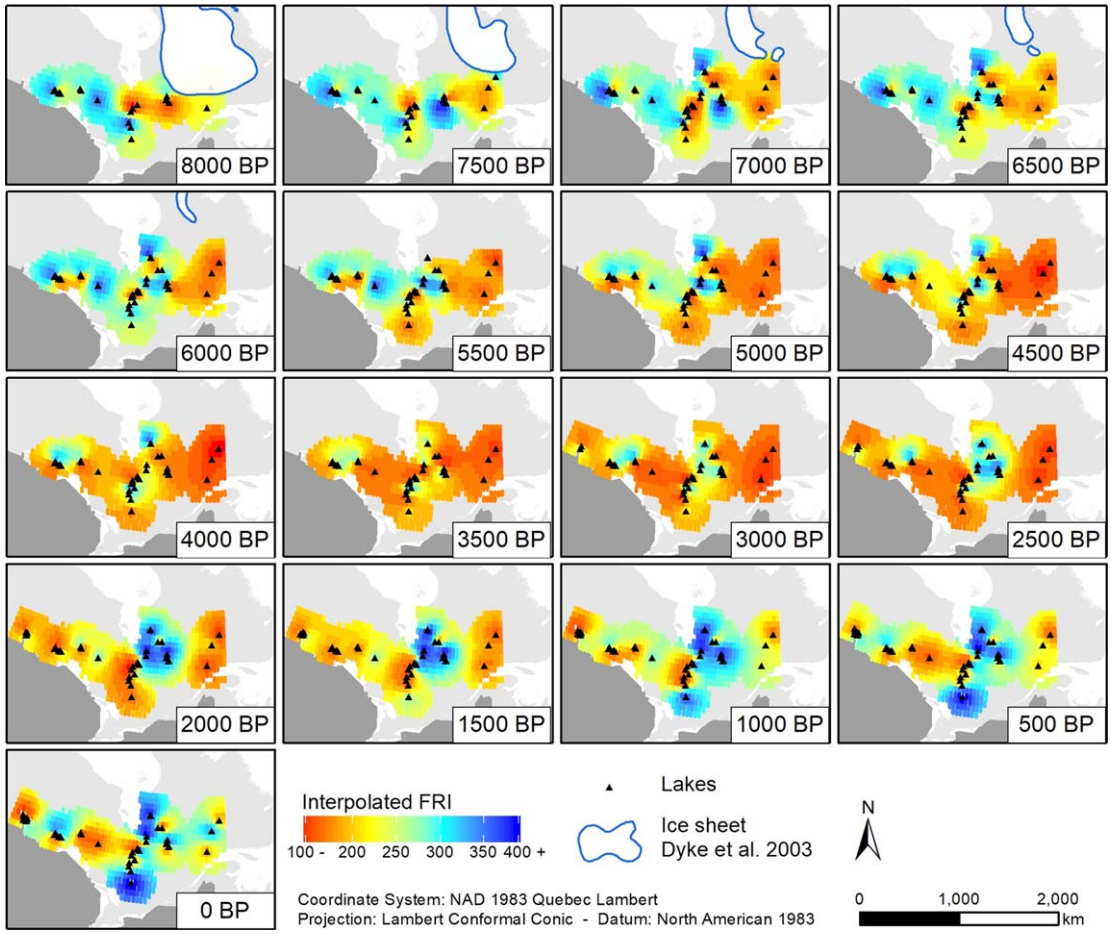

Figure 2. Spatial interpolation of the fire-return interval (FRI_{krig}) for 42 lakes from 8000 to 0 years before present (BP). Fire-return interval is defined as the elapsed time between two fires that are assumed to have occurred within a landscape area. FRI was extracted for each lake at 500 year intervals, and spatially interpolated using ordinary kriging. The estimated distribution of the Laurentian Ice sheet (Dyke *et al* 2003) is also illustrated using a conversion from radiocarbon estimated dates to calibrated calendar ages (Reimer *et al* 2013). Yellow to red colors indicate areas that experienced frequent fires.

temperature reconstruction and $CHAR_{krig}$ at each grid cell.

Results and discussion

Multi-millennial spatiotemporal variability in fire activity

Modern fire rotations (i.e. the time required to burn the equivalent of a specified area; period 1959–1999) range from 25 years to over 500 years across the study area (figure 1(a); Boulanger *et al* 2014). Of note is that the area has seen an increase in the proportion ($\hat{p}$) of its forests that have been affected by extreme biomass burning (i.e. area burned exceeded an empirical extreme detection threshold, see Data and Methods) during the AD 1980s, peaking in the early AD 1990s and then declining (figure 1(b); proportions were computed using the Canadian National Fire Database, hereafter $\hat{p}_{CNFD}$; see Data and Methods). This phenomenon was observed in analyses of both human-ignited and lightning-ignited fires (figure S7). The years 1988 and 1995, for example, had particularly high $\hat{p}_{CNFD}$ (respectively 52% and 57% of grid cells), distributed in all three provinces (figure S8).

We were interested in determining whether there were past analogs of such widespread biomass burning that could be reconstructed from lake-sediment charcoal records. We conducted spatially-interpolated reconstructions for the whole study area of the normalized charcoal ($CHAR_{krig}$) accumulation rate, which is representative of the amount of biomass burning, and of the mean FRI (FRI_{krig}), which is defined as the average time that has elapsed between successive fire events for a specified 0.5° × 0.5° grid cell during a specified 50 year time period.

Holocene distributions of FRI_{krig} (figure 2) and $CHAR_{krig}$ (figure 3) exhibited high variability through time. From *ca.* 8200 to 7800 BP, the study area experienced low FRI_{krig} and high biomass burning (figure 4). Following a period of fluctuating FRI_{krig}, low biomass burning lasted until about 6000 BP. FRI_{krig} was longer in the western sector and shorter in the eastern sector (figure 2). Between 6000 and 4500 BP, FRI_{krig} decreased and biomass burning increased (figure 2), as has been previously observed in North America (Hu *et al* 2006,

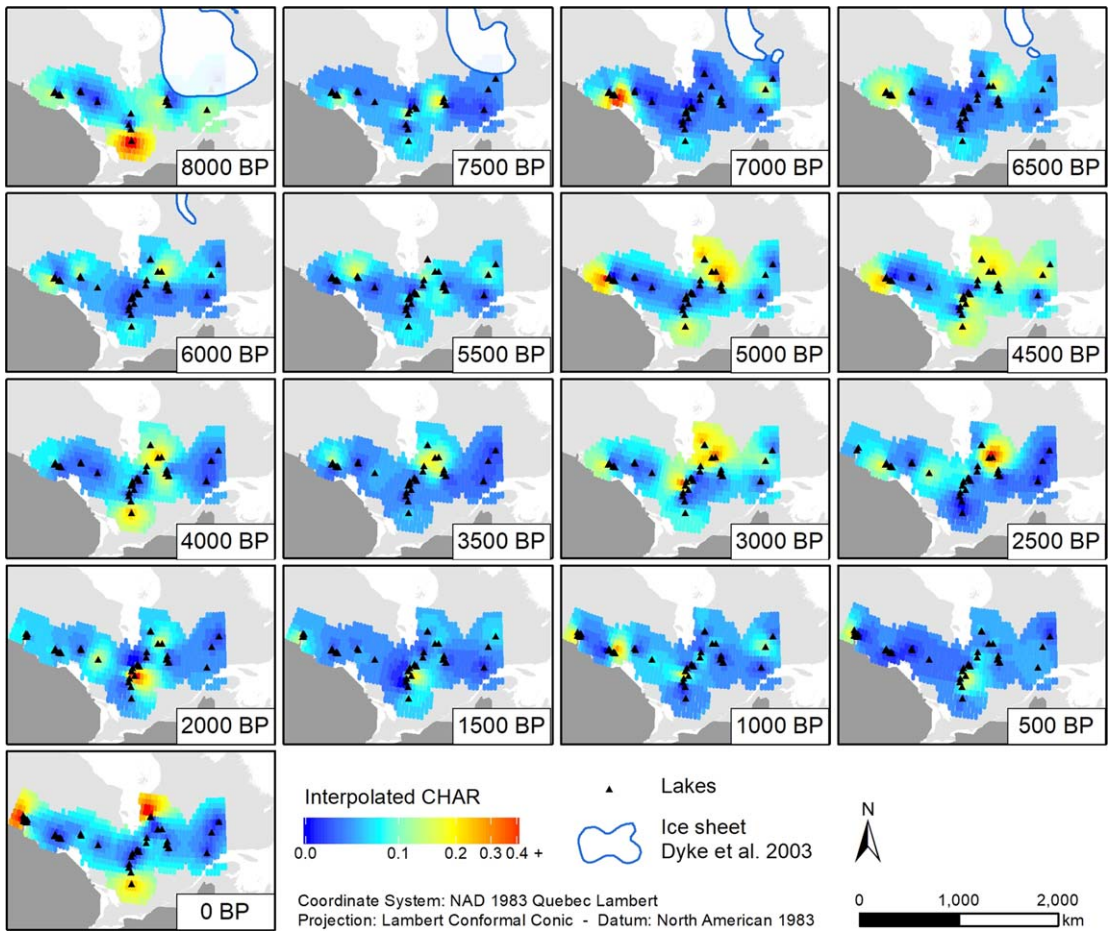

Figure 3. Spatial interpolation of normalized charcoal ($CHAR_{krig}$) accumulations for 42 lakes from 8000 to 0 years before present (BP). $CHAR_{krig}$ was extracted for each lake at 500 year intervals, and spatially interpolated using ordinary kriging. The estimated distribution of the Laurentian Ice sheet (Dyke *et al* 2003) is also illustrated using a conversion from radiocarbon estimated dates to calibrated calendar ages (Reimer *et al* 2013). Light blue to red colors indicate areas that underwent high biomass burning.

Ali *et al* 2009, Girardin *et al* 2013a). Between 4500 and 2500 BP, fire activity was at its highest (figures 2–4). The amount of biomass burning fluctuated but remained relatively high, on average (figure 4(c)). FRI_{krig} then gradually increased until 1000 BP, especially in the north-central part of the study area (figure 2), as has been shown by previous studies (Girardin *et al* 2013b, Blarquez *et al* 2015). From 1000 to 250 BP, FRI_{krig} also increased in the south-central part of the study area (figure 2), while remaining relatively high and constant elsewhere. During this period, biomass burning decreased. After 250 BP, we observed an increase in biomass burning and a decrease in FRI_{krig} (figure 4). A positive trend in biomass burning during 1750–1950 AD, roughly coinciding with the transition from the Pre-Industrial period to the Anthropocene (~1950 AD), was found across 49% of the area, but mostly limited to the western half (figure S9). Notable fluctuations in biomass burning since 1000 BP are broadly consistent with independent estimates of biomass burning emissions that were recently obtained from paleoatmospheric ethane in Greenland polar ice cores (figures 4(c) and S10; data from Nicewonger *et al* 2018). Biomass burning is one of two important sources of ethane in the preindustrial atmosphere (Nicewonger *et al* 2018). This demonstrates the relevance of the information that can be deduced from lake-sediment data for large-scale environmental issues: the correlation between the two independent records implies that fire activity in the study area is an important source for fire emissions transport into Greenland (Kehrwald *et al* 2012).

Embedded within this long-term variability are two periods of very-high biomass burning, each lasting about two centuries (figure 4(d)): from 4950 to 4750 BP and from 1250 to 1050 BP. In both cases, the $\hat{p}$ proportions of cells with $CHAR_{krig}$ values exceeding local extreme detection thresholds (hereafter $\hat{p}_{CHAR}$; see Data and Methods) were significantly elevated above overall background variability (figure 4(a)). These $CHAR_{krig}$ periods are not likely to be related to single large or severe fire events (i.e. biomass consumed per unit area), given that they occur simultaneously with decreases of FRI_{krig} (figure 4(a)). This observation implies that multiple fires marked both periods over the affected regions. During the period of 4950 to 4750 BP, $\hat{p}_{CHAR}$ covered 71% of the study area, mostly in the eastern sector (see inset maps of figure 4(d)). $CHAR_{krig}$ values also exceeded the

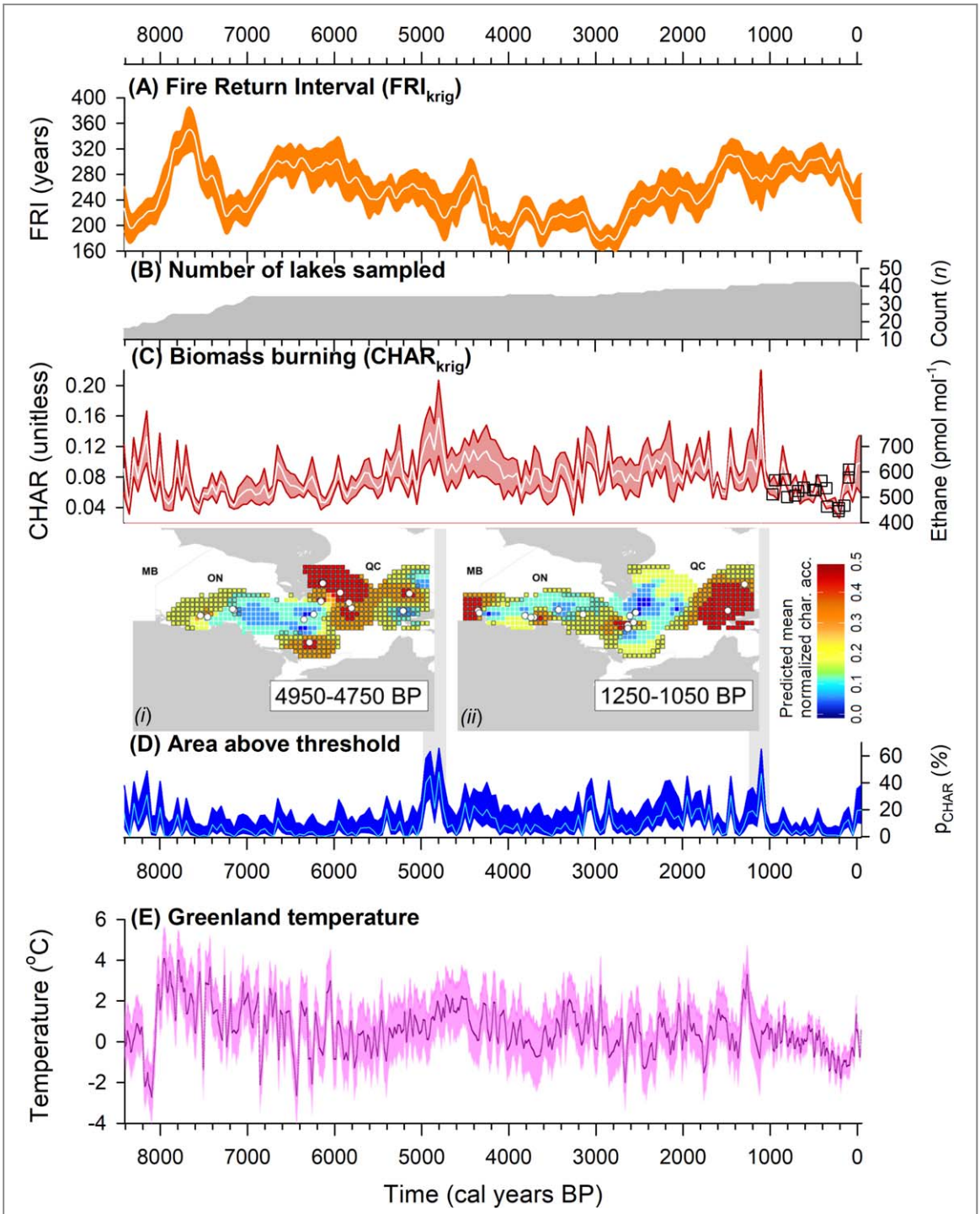

Figure 4. (a)–(c) Reconstructions of fire-return interval (FRI_{krig}) and biomass burning ($CHAR_{krig}$) averaged at the sub-continental scale. (a) FRI was extracted for each lake at 50 year intervals, spatially interpolated using ordinary kriging, and here averaged across the whole study area. The shading is indicative of the 95% confidence intervals (95% CI) for the averaged quantities, after adjusting the sample size to an effective degree of freedom. The number of lake-sediment charcoal records at a given time is shown in (b). (c) Same as (a) but for the normalized charcoal ($CHAR_{norm}$) accumulation. The squares illustrate the distribution of Greenland ice core ethane levels from (Nicewonger *et al* 2018) and are used as an independent fire proxy for benchmarking (also see figure S10 for a zoom of the last 1000 years). The two records are significantly correlated with $r = 0.62$ and bootstrap 95% CI [0.16, 0.86]. (d) Percent of the study area for which grid-cell $CHAR_{krig}$ exceeded locally-defined extreme detection thresholds at 50 year intervals ($\hat{p}_{CHAR}$), with 95% confidence intervals. The gray vertical bars delineate two periods during which a high percent of the study area underwent extreme biomass burning, i.e. 4950–4750 and 1250–1050 years BP. The inset maps show the distribution of those grid cells (outline in black) in which $CHAR_{krig}$ (color shading) exceeded extreme detection thresholds. Also, circles were added to illustrate the distribution of sampled lakes in which $CHAR_{interpolated}$ values, of the specified period, exceeded the extreme detection threshold specific to each lake. (e) Reconstructed mean annual Greenland temperatures, in anomalies relative to averages of 1951–1980, with 2 σ error (°C; Kobashi *et al* 2017).

detection threshold in 15 individual lake-sediment charcoal records (i.e. 45% of lakes) that were located in eastern and western parts of the study area (see inset maps of figure 4(d)). From 1250 to 1050 BP, $\hat{p}_{CHAR}$ covered 57% of the study area (figure 4(d)). $CHAR_{krig}$ values exceeding the threshold were also found in 15 of

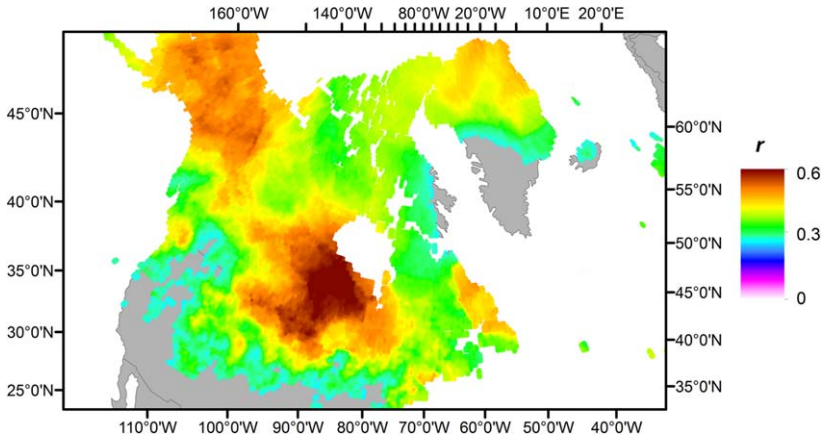

Figure 5. Correlation coefficient r between $\hat{p}_{CNFD}$ and gridded mean April–September temperature, 1959–2016. Orange to red colors indicate areas with high correlations. Areas in gray are not significant ($P > 0.05$).

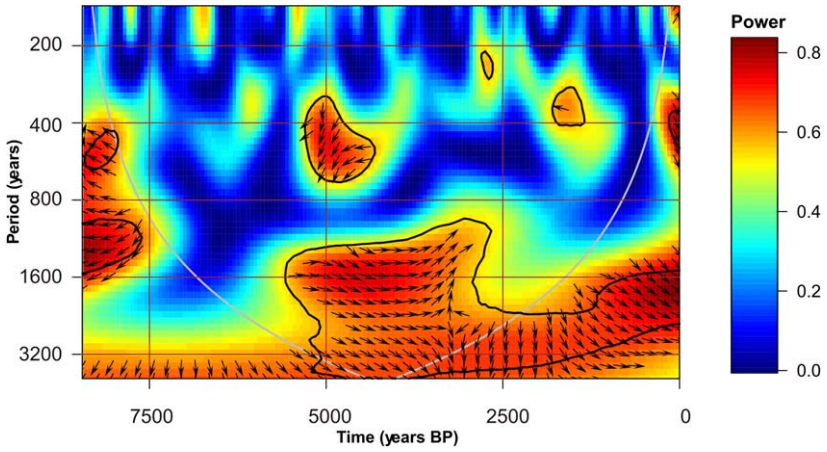

Figure 6. Wavelet coherence (WTC) between $\hat{p}_{CHAR}$ and the Greenland temperature reconstruction. Areas of large common power values in time and period (i.e. at a given time and periodicity in units of years) between $\hat{p}_{CHAR}$ and temperature data are shown in red. The 90% significance level against red noise is shown as a thick contour. The gray line delineates the 'cone of influence' where zero padding has reduced the variance. The relative phase relationship is shown by arrows, with in-phase pointing right, antiphase pointing left, temperature leading $\hat{p}_{CHAR}$ by 90° (1/4k) pointing down, and $\hat{p}_{CHAR}$ leading temperature by 90° (1/4k) pointing up. In-phase and antiphase relationships may be interpreted respectively as positive and negative correlations in time and period (Grinsted *et al* 2004).

the sampled lakes (38% of lakes; figure 4(d)). For this particular period, biomass burning occurred across many regions, stretching from the prairie-boreal ecotone to the easternmost boreal forests.

Aside from these two periods, the period 3100–2850 BP also stands out as having had a high fire activity (figure 4). In particular, we find FRIs among the lowest recorded. It should be noted that although an increase in $CHAR_{krig}$ occurred at the beginning of the Industrial Era, the proportion of cells exceeding the detection limit during the modern period was within the range of background variability (figure 4(d)).

Signatures of warming-induced extreme fire activity

Biomass burning is the result of additive effects of temperature, seasonal drought severity, duration of the snow-free period (equivalent to fire season length), and fuel availability (Molinari *et al* 2018, Chaste *et al* 2019). To our knowledge, evidence for a past-temperature influence on spatially widespread periods of high fire activity is lacking for our study area. To examine whether this effect was plausible, we analyzed the correlation between the metric $\hat{p}_{CNFD}$ during 1959–2016 (data from figure 1(b)) and April–September mean land temperatures (see Data and Methods). We found that $\hat{p}_{CNFD}$ co-varied in a positive manner with large-scale mean April–September warming at high latitudes, including over Greenland (figure 5). This positive covariance between fire-affected areas and Greenland temperature sets the basis for exploring relationships between past widespread boreal fire activity and multi-decadal temperature reconstructions covering the Holocene from Greenland ice cores (Kobashi *et al* 2017; figure 4(e)). Consistent with the analysis of modern fire and temperature data, wavelet coherence (WTC) analysis between the Greenland

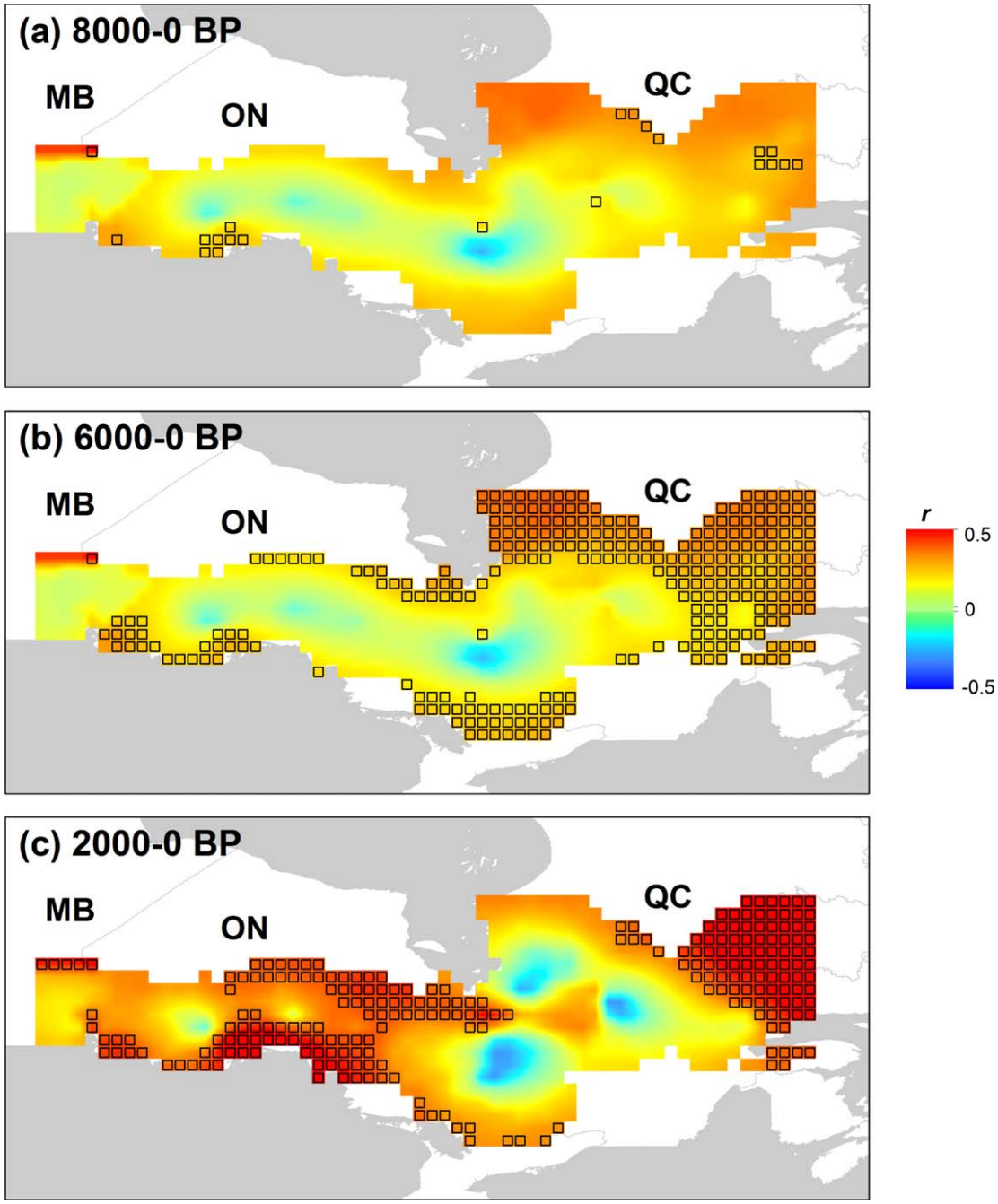

Figure 7. Correlation coefficient *r* between Greenland temperature reconstruction and gridded $CHAR_{krig}$ over periods (a) 8000–0 years BP, (b) 6000–0 years BP, and (c) 2000–0 yes BP. The maps were created from projecting correlation values that were computed at each grid point covered by the $CHAR_{krig}$ data and the Greenland temperature reconstruction. Orange to red colors indicate areas with high positive correlations; delineated areas are significant with $P < 0.05$ (determined from an effective degree of freedom for temporal autocorrelation in the data (von Storch and Zwiers 1999).

temperature reconstruction and the $\hat{p}_{CHAR}$ record indicated areas of significant and almost in-phase correlation at periodicities of >800 years per cycle since 6000 BP (i.e. $\hat{p}_{CHAR}$ generally lagging behind temperature; figure 6). High power was also noticeable during periods approximating those of high biomass burning, i.e. ~4250 to 5250 and ~1750 to 1250 BP at periodicities of about 400 years per cycle (albeit given the implied coarseness of the temporal resolution of the fire record, information that can be obtained is likely to be limited at such frequency). Non-parametric stationary bootstrapped correlations that were computed for the last 6000 years BP corroborated the WTC correlation for that period with $r = 0.20$ and 95% CI [0.05; 0.37] (about the same correlation was found between the global averages of $CHAR_{krig}$ values and Greenland temperature: $r = 0.24$ with 95%CI [0.04, 0.47]). Hence, $\hat{p}_{CHAR}$ significantly co-varied with Greenland temperature fluctuations, at least for the past 6000 years. The reason for low concordance between fire activity and the thermal maximum of 8000–6500 BP (Kobashi *et al* 2017, Bajolle *et al* 2018,

Porter *et al* 2019) remains to be elucidated. It could be hypothesized that relatively low biomass burning from 7500 to 6500 BP was the result of cold air masses associated with the remaining ice sheet in northern Quebec (Dyke 2004, Marsicek *et al* 2018, Liu *et al* 2014) (figures 1 and S13), humid conditions and high lake levels across large areas of eastern North America (Hély *et al* 2010, their figure 3(e)), and higher biomass of less fire-prone deciduous tree species, notably *Betula* and *Populus* (Girardin *et al* 2013a, Blarquez and Aleman 2016, figure S2). All these factors could have contributed to reduce spreading of crown fires.

It should be noted that the relationship between $CHAR_{krig}$ and temperature is not homogeneous across the study area (figure 7). It is a dominant feature of the easternmost sectors, and during the last 2000 years or so, it encompassed a larger part of the study area (figure 7(c), also see figures S11 and S12). Note also, that the pattern of temperature and $CHAR_{krig}$ correlation over the last 2000 years (figure 7(c)) is similar to the pattern of linear trends of $CHAR_{krig}$ from 200 to 0 BP (figure S9). It is likewise similar to the pattern of correlation between $\hat{p}_{CNFD}$ and gridded mean April-September temperatures for 1959–2016 (figure 5). From these observations, it appears to be a region in the center of the study area, southeast of James Bay, which emerges from the ensemble where $CHAR_{krig}$ temporal trajectories do not co-occur with high latitude temperatures. It was previously postulated that precipitation patterns and changes in the composition of forest landscapes were the main factors that would influence the fire activity trajectories below James Bay, as opposed to direct effects of warming on fire (Girardin *et al* 2009, 2013a). The decoupling of temperature and $CHAR_{krig}$ trajectories in that particular area adds credibility to this thesis.

Two periods of high sub-continental biomass burning and $\hat{p}_{CHAR}$ (i.e. 4950–4750 BP and 1250–1050 BP) are found during some of the periods of warmest Holocene temperatures in Greenland (respectively about +2.4 °C and +3.4 °C above the 1951–1980 baseline; figure 4(e); Kobashi *et al* 2017). Both periods coincide with positive temperature anomalies that have been inferred from chironomid assemblages in eastern boreal North American lakes (~+2.1 °C and 2.2 °C above baseline (Bajolle *et al* 2018, figure S11). Although the two high wildfire periods that have been identified herein had high temperatures in common, they developed under different precipitation and vegetation contexts. On one hand, the 4950–4750 BP episode occurred during a warm and dry period (Blarquez *et al* 2015, Karmakar *et al* 2015). On the other hand, the 1250–1050 BP episode occurred close to the short Medieval Climate Anomaly during a peak of high temperatures (PAGES 2k Consortium 2013, Kobashi *et al* 2017, Bajolle *et al* 2018, figure S11) within the otherwise cold and moist Neoglacial period (Viau and Gajewski 2009, Blarquez *et al* 2015, Karmakar *et al* 2015). To this may be added a third period, i.e. 3100–2850 BP and marked by low FRIs, which could fit into the warm anomaly of about 3400–2800 BP.

Our results covering past and modern times thus indicate that forest fires in the study area can be responsive to rapid warming at high latitudes. This is all the more important considering the changes that are currently underway in the North Atlantic basin. The $\hat{p}_{CNFD}$ exhibits a drop in 1992–1993, consistent with high-latitude cooling caused by the eruption of Mount Pinatubo (Parker *et al* 1996), followed by an increase until 2005 that is consistent with Greenland warming (figure S14). For the most recent 11 years on record (2005–2016), Greenland temperature has exhibited a slightly decreasing trend consistent with northern North Atlantic-wide cooling during that period (figure S15) and a slowdown of the Atlantic Ocean overturning circulation (Thornalley *et al* 2018). The proportion of forest that was affected by extreme biomass burning also declined during this period (figures 1 and S7). Clearly, a better understanding of the future decadal temperature variations in the Atlantic (e.g. Liu *et al* 2017) is of paramount importance in improving future boreal wildfire predictions in eastern boreal North America. Contextually, the spatial/temporal dimensions of warming and fire therein are likely to differ from other boreal regions of western North America where temperatures since the mid-20th century appear to be exceptionally warm in comparison with the last 13 000 years (Marsicek *et al* 2018; Porter *et al* 2019).

Conclusion

Our retrospective analysis, which was based upon a network of lake-sediment charcoal records, allowed us to identify two periods of widespread biomass burning across eastern North American boreal forests at 4950–4750 BP and 1250 to 1050 BP. Both periods coincided with positive temperature anomalies over Greenland (+2 °C to +3 °C above baseline) and are likely the best analogs for what could be anticipated in terms of impacts on fire in coming decades (mid-century) across much of eastern boreal North America as a consequence of human-caused climate changes (approximately +2 °C to +4 °C above the 1951–1980 baseline by 2040 for that particular area according to Chaste *et al* 2019). On the other hand, it is not to be ruled out that end-of-this-century conditions could exceed anything experienced in the Holocene (including the warm early-mid Holocene) and that the best analogs could likely come from more ancient periods (Burke *et al* 2018). We recommend that future studies aiming at clarifying the spatial/temporal dimensions of a high fire period in the past focus on very-high resolution charcoal and pollen collections targeting the sediment horizons spanning such events. Their detailed documentation could provide valuable insights regarding the effects of widespread burning on vegetation composition, boreal

forest dynamics, and the carbon cycle. The capacity of boreal conifer tree species to maintain themselves, for boreal carbon stocks to recover, and for ecosystem services to be maintained in face of multiple fire disturbances could be better evaluated on the basis of these empirical data. This would also offer new opportunities to benchmark dynamic global vegetation model simulations. Such comprehensive analysis of past climate change impacts on fire activity, including past warm periods, is needed to inform future predictions of how changes in extreme wildfires could transform existing forest ecosystems (Sankey 2018).

Acknowledgments

This work was made possible thanks to financial support from the Strategic Grant and Discovery Programs of the Natural Sciences and Engineering Research Council of Canada (NSERC), and the Canadian Forest Service. We thank William J Parsons for the editing of the manuscript, and two anonymous reviewers for their comments on an earlier version.

Data availability statement

The data that support the findings of this study are available from the corresponding author upon reasonable request.

ORCID iDs

Martin P Girardin https://orcid.org/0000-0003-0436-7486
Jeanne Portier https://orcid.org/0000-0002-9706-5155
Cécile C Remy https://orcid.org/0000-0003-1231-0498
Hugo Asselin https://orcid.org/0000-0002-9542-4994
Sylvie Gauthier https://orcid.org/0000-0001-6720-0195
Yves Bergeron https://orcid.org/0000-0003-3707-3687

References

Ali A A, Carcaillet C and Bergeron Y 2009 Long-term fire frequency variability in the eastern Canadian boreal forest: the influences of climate versus local factors *Glob. Change Biol.* **15** 1230–41

Ansmann A, Baars H, Chudnovsky A, Mattis I, Veselovskii I, Haarig M, Seifert P, Engelmann R and Wandinger U 2018 Extreme levels of Canadian wildfire smoke in the stratosphere over central Europe on 21–22 August 2017 *Atmos. Chem. Phys.* **18** 11831–45

Bajolle L, Larocque-Tobler I, Gandouin E, Lavoie M, Bergeron Y and Ali A A 2018 Major postglacial summer temperature changes in the central coniferous boreal forest of Quebec (Canada) inferred using chironomid assemblages *J. Quat. Sci.* **33** 409–20

Blaauw M 2010 Methods and code for 'classical' age-modelling of radiocarbon sequences *Quat. Geochronol.* **5** 512–8

Blarquez O and Aleman J C 2016 Tree biomass reconstruction shows no lag in postglacial afforestation of eastern Canada *Can. J. For. Res.* **46** 485–98

Blarquez O, Ali A A, Girardin M P, Grondin P, Fréchette B, Bergeron Y and Hély C 2015 Regional paleofire regimes affected by non-uniform climate, vegetation and human drivers *Sci. Rep.* **5** 13356

Boulanger Y, Gauthier S and Burton P J 2014 A refinement of models projecting future Canadian fire regimes using homogeneous fire regime zones *Can. J. For. Res.* **44** 365–76

Bowman D M J S, Williamson G J, Abatzoglou J T, Kolden C A, Cochrane M A and Smith A M S 2017 Human exposure and sensitivity to globally extreme wildfire events *Nat. Ecol. Evol.* **1** 1–6

Bowman D M J S *et al* 2011 The human dimension of fire regimes on Earth *J. Biogeogr.* **38** 2223–36

Brossier B, Oris F, Finsinger W, Asselin H, Bergeron Y and Ali A A 2014 Using tree-ring records to calibrate peak detection in fire reconstructions based on sedimentary charcoal records *Holocene* **24** 635–45

Brown L D, Cai T T and DasGupta A 2001 Interval estimation of binomial proportion *Stat. Sci.* **16** 101–17

Burke K D, Williams J W, Chandler M A, Haywood A M, Lunt D J and Otto-Bliesner B L 2018 Pliocene and Eocene provide best analogs for near-future climates *Proc. Natl Acad. Sci.* **115** 13288–93

Chaste E, Girardin M P, Kaplan J O, Bergeron Y and Hély C 2019 Increases in heat-induced tree mortality could drive reductions of biomass resources in Canada's managed boreal forest *Landsc. Ecol.* **34** 403–26

Cowtan K and Way R G 2014 Coverage bias in the HadCRUT4 temperature series and its impact on recent temperature trends *Q. J. R. Meteorol. Soc.* **140** 1935–44

Cressie N 1990 The origins of kriging *Math. Geol.* **22** 239–52

Cyr D, Gauthier S, Bergeron Y and Carcaillet C 2009 Forest management is driving the eastern North American boreal forest outside its natural range of variability *Front. Ecol. Environ.* **7** 519–24

Dale M R T and Fortin M-J 2002 Spatial autocorrelation and statistical tests in ecology *Ecoscience* **9** 162–7

Delignette-Muller M-L and Dutang C 2015 fitdistrplus : An R Package for fitting distributions *J. Stat, Softw.* **64** 1–84

Dyke A S 2004 An outline of North American deglaciation with emphasis on central and northern Canada *Quaternary Glaciations-Extent and Chronology, Part II: North America* vol 2 (Amsterdam: Elsevier) pp 373–424

Dyke A S, Moore A and Robertson L 2003 Deglaciation of North America, Open File 1574 (Ottawa, Canada: Geological Survey of Canada) (https://doi.org/10.4095/214399)

Erni S, Arseneault D, Parisien M-A and Bégin Y 2017 Spatial and temporal dimensions of fire activity in the fire-prone eastern Canadian taiga *Glob. Change Biol.* **23** 1152–66

Flannigan M D, Krawchuk M A, De Groot W J, Wotton B M and Gowman L M 2009 Implications of changing climate for global wildland fire *Int. J. Wildl. Fire* **18** 483–507

Gauthier S, Bernier P, Kuuluvainen T, Shvidenko A Z and Schepaschenko D G 2015 Boreal forest health and global change *Science* **349** 819–22

Gavin D G, Hu F S, Lertzman K and Corbett P 2006 Weak climatic control of stand-scale fire history during the Late Holocene *Ecology* **87** 1722–32

Girardin M P, Ali A A, Carcaillet C, Blarquez O, Hély C, Terrier A, Genries A and Bergeron Y 2013a Vegetation limits the impact of a warm climate on boreal wildfires *New Phytol.* **199** 1001–11

Girardin M P, Ali A A, Carcaillet C, Gauthier S, Hély C, Le Goff H, Terrier A and Bergeron Y 2013b Fire in managed forests of eastern Canada: risks and options *For. Ecol. Manage.* **294** 238–49

Girardin M P, Ali A A, Carcaillet C, Mudelsee M, Drobyshev I, Hély C and Bergeron Y 2009 Heterogeneous response of circumboreal wildfire risk to climate change since the early 1900s *Glob. Change Biol.* **15** 2751–69

Gouhier T C, Grinsted A and Gouhier M T C 2018 Package 'biwavelet': conduct Univariate and Bivariate Wavelet Analyses (https://cran.r-project.org/web/packages/biwavelet/biwavelet.pdf)
Grinsted A, Moore J C and Jevrejeva S 2004 Application of the cross wavelet transform and wavelet coherence to geophysical time series *Nonlinear Process. Geophys. Eur. Geosci. Union* **11** 561–6
Hampel F R 1985 The breakdown point of the mean combined with some rejection rules *Technometrics* **27** 95–107
Hély C, Girardin M P, Ali A A, Carcaillet C, Brewer S and Bergeron Y 2010 Eastern boreal North American wildfire risk of the past 7000 years: a model-data comparison *Geophys. Res. Lett.* **37** L14709
Heyerdahl E K, Mckenzie D, Daniels L D, Hessl A E, Littell J S and Mantua N J 2008 Climate drivers of regionally synchronous fires in the inland Northwest (1651–1900) *Int. J. Wildl. Fire* **17** 40–9
Hiemstra P, Pebesma E J, Twenhöfel C J W and Heuvelink G B M 2009 Real-time automatic interpolation of ambient gamma dose rates from the Dutch radioactivity monitoring network *Computers and Geosciences* **35** 1711–21
Higuera P E, Chipman M L, Barnes J L, Urban M A and Hu F S 2011 Variability of tundra fire regimes in Arctic Alaska: millennial-scale patterns and ecological implications *Ecol. Appl.* **21** 3211–26
Higuera P E, Gavin D G, Bartlein P J and Hallett D J 2010 Peak detection in sediment—charcoal records : impacts of alternative data analysis methods on fire-history interpretations *Int. J. Wildl. Fire* **19** 996–1014
Higuera P E, Sprugel D G and Brubaker L B 2005 Reconstructing fire regimes with charcoal from small-hollow sediments: a calibration with tree-ring records of fire *Holocene* **15** 238–51
Hu F S, Brubaker L B, Gavin D G, Higuera P E, Lynch J A, Rupp T S and Tinner W 2006 How climate and vegetation influence the fire regime of the Alaskan boreal biome: the holocene perspective *Mitig. Adapt. Strateg. Glob. Change* **11** 829–46
Hu Q *et al* 2018 A study of long-range transported smoke aerosols in the Upper Troposphere/Lower Stratosphere *Atmos. Chem. Phys.* **19** 1173–93
Hua Q, Barbetti M and Rakowski A Z 2013 Atmospheric radiocarbon for the period 1950–2010 *Radiocarbon* **55** 2059–72
Jain P, Wang X and Flannigan M D 2017 Trend analysis of fire season length and extreme fire weather in North America between 1979 and 2015 *Int. J. Wildl. Fire* **26** 1009–20
Johnson E A and Gutsell S L 1994 Fire frequency models, methods and interpretations *Adv. Ecol. Res.* **25** 239–87
Karmakar M, Laird K R and Cumming B F 2015 Diatom-based evidence of regional aridity during the mid-Holocene period in boreal lakes from northwest Ontario (Canada) *Holocene* **25** 166–77
Kehrwald N, Zangrando R, Gabrielli P, Jaffrezo J L, Boutron C, Barbante C and Gambaro A 2012 Levoglucosan as a specific marker of fire events in Greenland snow *Tellus* B **64** 18196
Kelly R F, Higuera P E, Barrett C M and Hu F S 2011 Short paper: a signal-to-noise index to quantify the potential for peak detection in sediment–charcoal records *Quat. Res.* **75** 11–7
Kobashi T *et al* 2017 Volcanic influence on centennial to millennial Holocene Greenland temperature change *Sci. Rep.* **7** 1–10
Krezek-Hanes C C, Ahern F, Cantin A and Flannigan M D 2011 Trends in large fires in Canada, 1959–2007. Canadian biodiversity: ecosystem Status and Trends 2010 *Technical Thematic Report No.* 6 (Ottawa, ON: Northern Forestry Centre)
Landis M S, Edgerton E S, White E M, Wentworth G R, Sullivan A P and Dillner A M 2018 The impact of the 2016 Fort McMurray Horse River Wildfire on ambient air pollution levels in the Athabasca Oil Sands Region, Alberta, Canada *Sci. Total Environ.* **618** 1665–76
Liu W, Xie S-P, Liu Z and Zhu J 2017 Overlooked possibility of a collapsed Atlantic Meridional Overturning Circulation in warming climate *Sci. Adv.* **3** e1601666
Liu Z, Lu Z, Wen X, Otto-Bliesner B L, Timmermann A and Cobb K M 2014 Evolution and forcing mechanisms of El Niño over the past 21,000 years *Nature* **515** 550–3
Marlon J R *et al* 2012 Long-term perspective on wildfires in the western USA *Proc. Natl Acad. Sci.* **109** E535–43
Marsicek J, Shuman B N, Bartlein P J, Shafer S L and Brewer S 2018 Reconciling divergent trends and millennial variations in Holocene temperatures *Nature* **554** 92–6
Molinari C, Lehsten V, Blarquez O, Carcaillet C, Davis B A S, Kaplan J O, Clear J and Bradshaw R H W 2018 The climate, the fuel and the land use: Long-term regional variability of biomass burning in boreal forests *Glob. Change Biol.* **24** 4929–45
Moore J, Grinsted A and Jevrejeva S 2007 Evidence from wavelet lag coherence for negligible solar forcing of climate at multi-year and decadal periods *Nonlinear Dynamics in Geosciences* (New York, NY: Springer) pp 457–64
Mudelsee M 2003 Estimating Pearson's correlation coefficient with bootstrap confidence interval from serially dependent time series *Math. Geol.* **35** 651–65
Natural Resources Canada 2018 The state of Canada's forests *Annual Report 2018* (Ottawa: Natural Resources Canada, Canadian Forest Service)
Nicewonger M R, Aydin M, Prather M J and Saltzman E S 2018 Large changes in biomass burning over the last millennium inferred from paleoatmospheric ethane in polar ice cores *Proc. Natl Acad. Sci.* **115** 12413–8
Oris F, Asselin H, Ali A A, Finsinger W and Bergeron Y 2014 Effect of increased fire activity on global warming in the boreal forest *Environ. Rev.* **22** 206–19
PAGES 2k Consortium 2013 Continental-scale temperature variability during the past two millennia *Nat. Geosci.* **6** 339–46
Parker D E, Wilson H, Jones P D, Christy J R and Folland C K 1996 The impact of Mount Pinatubo on world-wide temperatures *Int. J. Climatol.* **16** 487–97
Parnell A C, Haslett J, Allen J R M, Buck C E and Huntley B 2008 A flexible approach to assessing synchroneity of past events using Bayesian reconstructions of sedimentation history *Quat. Sci. Rev.* **27** 1872–85
Pellatt M G, McCoy M and Mathewes R W 2015 Paleoecology and fire history of garry oak ecosystems in canada: implications for conservation and environmental management *Biodivers. Conserv.* **24** 1621–39
Porter T J, Schoenemann S W, Davies L J, Steig E J, Bandara S and Froese D G 2019 Recent summer warming in northwestern Canada exceeds the Holocene thermal maximum *Nat. Commun.* **10** 1631
R Core Team 2014 *R: A language and environment for statistical computing* (Vienna, Austria: R Foundation for Statistical Computing) (http://R-project.org/)
Reimer P J *et al* 2013 IntCal13 and Marine13 radiocarbon age calibration curves 0–50 000 years cal BP *Radiocarbon* **55** 1869–87
Sankey S 2018 *Blueprint for wildland fire science in Canada (2019–2029)* (Edmonton, Alberta: Natural Resources Canada, Canadian Forest Service, Northern Forestry Centre)
San-Miguel-Ayanz J, Durrant T, Boca R, Libertà G, Branco A, de Rigo D, Ferrari D, Maianti P, Artés Vivancos T, Oom D, Pfeiffer H, Nuijten D and Leray T 2018 Forest Fires in Europe, Middle East and North Africa 2018 (Italy: Joint Research Centre, European Commission, Ispra (VA)) (https://doi.org/10.2760/1128)
Statistics Canada 2017 Infographic: Fort McMurray 2016 Wildfire —Economic Impact. (Ottawa, ON: Statistics Canada)
Stocks B J *et al* 2002 Large forest fires in Canada, 1959–1997 *J. Geophys. Res.* **108** 8149
Thornalley D J R *et al* 2018 Anomalously weak Labrador Sea convection and Atlantic overturning during the past 150 years *Nature* **556** 227–30
van Oldenborgh G J, Coelho C A S and Doblas-Reyes F J 2008 Exploratory analysis and verification of seasonal forecasts with the KNMI climate explorer *ECMWF Newsl.* **116** 4–5

Viatte C, Strong K, Paton-Walsh C, Mendonca J, O'Neill N T and Drummond J R 2013 Measurements of CO, HCN, and C2H6 total columns in smoke plumes transported from the 2010 Russian boreal forest fires to the Canadian High Arctic *Atmos. Ocean* **51** 522–31

Viau A E and Gajewski K 2009 Reconstructing millennial-scale, regional paleoclimates of boreal Canada during the holocene *J. Clim.* **22** 316–30

von Storch H and Zwiers F W 1999 *Statistical Analysis in Climate Research* (Cambridge: Cambridge University Press) (https://doi.org/10.1017/CBO9780511612336)

Waito J, Girardin M P, Tardif J C, Conciatori F, Bergeron Y and Ali A A 2018 Recent fire activity in the boreal eastern interior of North America is below that of the past 2000 yr *Ecosphere* **9** e02287

Waito J, Girardin M P, Tardif J C, Hély C, Blarquez O and Ali A A 2015 Fire and climate: using the past to predict the future *Routledge Handbook of Forest Ecology* (London: Routledge) pp 489–503

Walker M *et al* 2018 Formal ratification of the subdivision of the Holocene Series/Epoch (Quaternary System/Period): two new Global Boundary Stratotype sections and Points (GSSPs) and three new stages/ subseries *Episodes* **41** 213–23

Wang Y, Goring S J and McGuire J L 2019 Bayesian ages for pollen records since the last glaciation in North America *Sci. Data* **6** 176

Wotton B M, Flannigan M D and Marshall G A 2017 Potential climate change impacts on fire intensity and key wildfire suppression thresholds in Canada environ *Res. Lett.* **12** 095003